are assumed small and have been neglected. For the data presented the major axis was always very close to the sample plate normal, so that much of the structure in the R_{ij} curves occurs for angles considerably less than 12°. A three-dimensional solution to the boundary-value problem would clarify the effects of tipping.

This paper presents the most complete study thus far of resistivity tensor elements using the helicon technique. The helicon method offers several advantages over conventional dc techniques. No leads need be attached to the sample, and the instrumentation is relatively inexpensive and straightforward to use. High resolution is possible in dc experiments as shown by the work of Klauder *et al.*[2] in copper. Comparable results are possible with the helicon method in metals of comparable purity. The helicon method has the disadvantage of requiring the solution of a boundary-value problem.

---

*Work supported in part by the Research Corporation, the U.S. Atomic Energy Commission [Contract No. AT (30-1)-4186] and the Samuel P. Hunt Foundation.

†Present address: Department of Engineering and Applied Science, Yale University, New Haven, Conn.

[1]I. M. Lifschitz, M. I. Azbel, and M. I. Kaganov, Zh. Eksperim. i Teor. Fiz. 31, 63 (1956) [Soviet Phys. JETP 4, 41 (1957)]; E. Fawcett, Advan. Phys. 13, 139 (1964).

[2]N. E. Alekseevskii and Yu. P. Gaidukov, Zh. Eksperim. i Teor. Fiz. 42, 69 (1962) [Soviet Phys. JETP 15, 49 (1962)]. For dc measurements of resistivity tensor elements in copper, see J. R. Klauder, W. A. Reed, G. F. Brennert, and J. E. Kunzler, Phys. Rev. 141, 592 (1966).

[3]R. G. Chambers and B. K. Jones, Proc. Roy. Soc. (London) A270, 417 (1962); P. A. Penz, J. Appl. Phys. 38, 4047 (1967).

[4]J. R. Merrill, Phys. Rev. 166, 716 (1968).

[5]M. T. Taylor, J. R. Merrill, and R. Bowers, Phys. Rev. 129, 2525 (1963).

[6]J. R. Merrill, M. T. Taylor, and J. M. Goodman, Phys. Rev. 131, 2499 (1963).

[7]J. R. Klauder and J. E. Kunzler, Phys. Rev. Letters 6, 179 (1961).

[8]S. W. Hui, J. Appl. Phys. 40, 3521 (1969).

[9]S. J. Buchsbaum and P. A. Wolff, Phys. Rev. Letters 15, 406 (1965).

[10]C. R. Legendy, Phys. Rev. 135, A1713 (1964).

PHYSICAL REVIEW B VOLUME 2, NUMBER 4 15 AUGUST 1970

Electronic Structure Effects in the Drude and Interband Absorption of Aluminum*

David Brust

Lawrence Radiation Laboratory, University of California, Livermore, California 94550

(Received 5 March 1970)

Using Ashcroft's potential, the interband and Drude absorption in aluminum have been calculated. Two large peaks occur in the interband part of $\epsilon_2(\omega)$ at 0.5 and 1.6 eV. In addition, the interband absorption continues as $\hbar\omega \to 0$. The optical effective mass is calculated with the result that $m_a^* = 1.45\, m_0$. Comparison with experiment is excellent. It is concluded that the optical spectrum of aluminum is completely understood in terms of the band structure. It is also pointed out that the optical peaks can be used to help determine the Fermi surface.

INTRODUCTION

Among the simple metals, aluminum is one of the most interesting from the point of view of electronic theory. This is due, in large part, to the success of the nearly free-electron (NFE) model in interpreting Fermi-surface experiments.[1,2] In this regard, Ashcroft[2] has shown that a simple two-parameter pseudopotential will account very nicely for the small departure from a completely free-electron picture.

Since the band structure of aluminum is expected to be well described by NFE model, one would hope to be in a position to account for its optical properties. The picture, however, is somewhat unclear. On the experimental side, optical response functions have been studied in the infrared and optical regimes by many investigators over the past few years.[3–12] Using the data available to them, Ehrenreich *et al.*[13] constructed the real and imaginary parts of the dielectric function. Using the infrared portion of the curves,

they found an effective mass m_a^* and lifetime τ which account for the Drude contribution. Subtracting the Drude term, they also deduced the interband part of $\epsilon_2(\omega)$. Their subsequent analysis based on Segall's band calculations[14] resulted in two puzzles. First of all, the empirical value of m_a^* was found $\approx 1.50\ m_0$. The band-theoretic value, on the other hand, was found $\approx 1.15\ m_0$, quite close to the free-electron value. Second, they found an experimental peak in $\epsilon_2(\omega)$ near 1.6 eV. This was related to interband transitions, but the computed intensity was too small by a factor of at least 3. In that paper, the authors pointed out that one might explain both discrepancies by a transfer of oscillator strength from the intraband modes to the interband modes. Electron-electron interactions were suggested as a possible source for the spectral weight shift.

The present investigation was undertaken for the express purpose of determining whether the NFE model is quantitatively capable of reproducing the optical response functions of aluminum. If the model is to be meaningful, it must reproduce simultaneously the Fermi-surface data. The latter demand is met by choosing Ashcroft's potential.

Having settled on the potential, the Brillouin zone is studied so that the interband absorption may be accurately determined. Surprisingly, it proves to require a more detailed calculation to get the interband contribution for a NFE polyvalent metal than for an insulator. This is due, in part, to the rapid variation of the dipole matrix element with crystal momentum and in part to the additional reasons discussed below.

The calculation of the Drude term hinges on an accurate evaluation of m_a^*. Since the effective mass depends only on the band-structure properties at the Fermi surface, it would be surprising indeed if the Ashcroft potential failed to give this quantity correctly. Any discrepancy between the empirical value and the band-theoretic value would have to be attributed to many-particle effects. One would hope, however, that quasiparticle screening is sufficiently good in aluminum to keep these corrections small vis-à-vis the optical response functions. Fortunately, our present calculation gives a value of $m_a^* = 1.45\ m_0$. The large deviation from the free-electron value is caused by contact of the Fermi sea with the zone boundaries. The accurate determination of m_a^* is done by a simple method outlined in the body of this paper.

It is shown that the theory gives a good account of the experiment if an empirical lifetime parameter is introduced into the calculation. Good agreement is found in the far-infrared range where the Drude absorption dominates. A novel feature of our study is the demonstration that interband absorption continues as $\hbar\omega \to 0$. It is negligible in comparison with the free-electron part below ~ 0.4 eV, except in the limit $\tau \to \infty$, where it gradually dominates at all frequencies (other than $\hbar\omega = 0$).

In the middle and near infrared, two peaks are found. The two peaks are related to interband-absorption effects which are understood by consideration of the free-electron-like energy bands. A result of particular interest to Fermi-surface studies is that the positions of the two peaks are nearly exactly equal to $2|V(3)|$ and $2|V(4)|$, respectively. Thus a knowledge of the position of these two peaks is sufficient to work backward to the Fermi surface.

The tail region of the curve which extends through the visible range is in perfect accord with experiment. This portion of the curve is almost entirely due to interband effects.

ENERGY BANDS

Computational Procedures

Ashcroft[2] originally constructed his potential to give an optimum fit to the Fermi-surface data in aluminum. It is adopted here to compute the entire band structure. Thus, the potential coefficients are $V(3) = 0.0179$ Ry, $V(4) = 0.0562$ Ry, and all other $V(K) = 0.0$. Actually, small energy-dependent corrections are required if one wishes to compute the entire band structure over an energy range ~ 20 eV. Direct comparison with first-principles augmented-plane-wave (APW) studies[15] shows these corrections to be less than 5%. The comparison suggests that a reasonable approximation to the energy-dependent terms is achieved by increasing the free-electron mass $\sim 4\%$ where it appears on the diagonal of the secular equation. This is equivalent to increasing the lattice constant by 2% in calculating the band structure. Inclusion of this weak energy dependence has a rather small effect on the results of our present study. This is especially true as we are primarily interested in states within 3–4 eV of the Fermi surface.

The next consideration is the secular equation dimension. Examination of the free-electron bands suggests that either four, nine, or thirteen plane waves be used in the $\frac{1}{48}$th irreducible volume of the Brillouin zone. A glance at Table I indicates that one can expect convergence errors up to 0.3 eV with the 4×4 secular equation size. This was judged to be intolerable. The 9×9, however, appears to give convergence ~ 0.1 eV and was used for the calculation. One should bear in mind that using a fixed number of

TABLE I. The energy shifts (in eV) relative to the Fermi level of several eigenvalues as a function of the number of plane waves in the expansion.

Level	Number of plane waves 4	9	13	~125[a]
$\Delta X_4'$	−0.09	−0.05	−0.04	0.0
ΔX_1	+0.12	+0.07	+0.06	0.0
ΔW_3	−0.08	−0.05	−0.05	0.0
$\Delta W_{2'}$	+0.01	+0.01	+0.01	0.0
ΔW_1	+0.30	+0.12	+0.06	0.0
ΔK_3	−0.08	−0.05	−0.04	0.0
ΔK_1	−0.02	+0.01	+0.01	0.0
ΔK_1	+0.19	+0.06	+0.01	0.0

[a]The last column includes a number of states through the use of the perturbation theory and is taken as the convergence limit.

plane waves results in symmetry breaking of the band structure. This is negligible, however, with the 9×9 secular equation. In addition, experiments were performed with the effect of higher potential coefficients on the band structure, guided, in this respect, by the Animalu-Heine[16] model potential for the tail part of $V(K)$. The effect of these coefficients on the band structure is also negligible, being less than the convergence errors. The complete band diagram for the symmetry directions is drawn in Fig. 1. It is quite similar to those of other calculations.[1, 14, 15, 17]

Density of States and Fermi Level

Establishment of a band structure was followed by the derivation of the concomitant density of states. In order to do this, energy eigenvalues were computed about 2000 inequivalent points in the $\frac{1}{48}$th portion of the zone. Then additional eigenvalues were computed by quadrically interpolating between these points. In all, eigenvalues were computed at an additional 1 100 000 inequivalent points this way. This large sample was generated by a Monte Carlo procedure. Figure 2 shows the density of states. The lower-energy portion of the curve is quite parabolic. As the energy at the first zone boundary is approached, the deviations from free-electron behavior become noticeable. The L point, however, produces only a very slight distortion in the density of states. We note that the Fermi level is lower than the free-electron Fermi energy value by about $\frac{1}{2}$ eV. This is due mainly to the energy dependence of the potential.

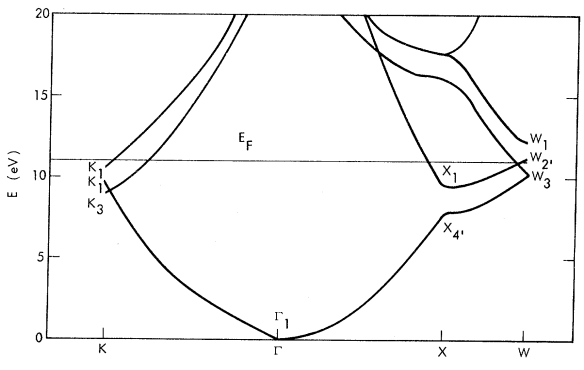

FIG. 1. Energy bands of aluminum using Ashcroft's potential.

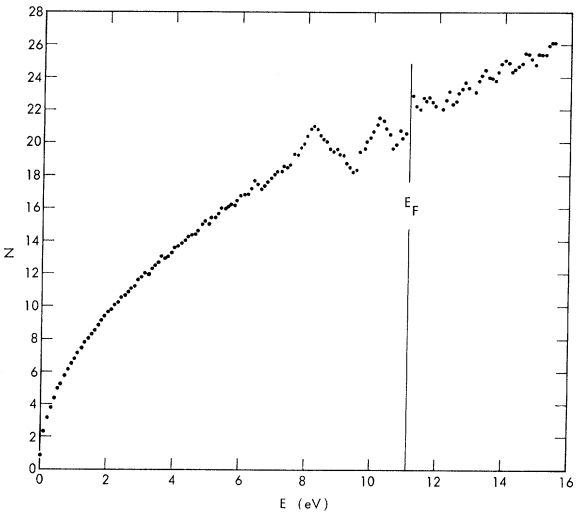

FIG. 2. Aluminum density of states in arbitrary units.

INTERBAND CONTRIBUTIONS TO DIELECTRIC CONSTANT $\tau = 0$

For a metal, a complete discussion of the frequency-dependent dielectric functions requires an analysis of both intraband and interband contributions. In this section the latter is discussed. The imaginary part of $\epsilon(\omega)$ within the random-phase approximation neglects the lifetime broadening[18]:

$$\epsilon_2^b(\omega) = \frac{1}{3}\frac{4\pi e^2}{m_0}\sum_{\vec{k},n,s}\frac{\pi}{2\omega}H[E_n(\vec{k})-E_F]H \times[E_F - E_s(\vec{k})]f_{ns}(\vec{k})\delta[\omega-\omega_{ns}(\vec{k})] \quad . \qquad (1)$$

In Eq. (1), the superscript b stands for "the interband contribution of." $H(X)$ is defined according to the usual convention

$$H(X) = 1 \text{ if } X \geq 0$$
$$= 0 \text{ if } X < 0 \quad . \qquad (2)$$

$H(X)$ is simply the $T = 0°$ limit of the Fermi-Dirac function. In Eq. (1), $f_{ns}(\vec{k})$ is the standard oscil-

lator-strength function

$$f_{ns}(\vec{k}) = 2|\vec{P}_{ns}(\vec{k})|^2/\hbar m_0 \omega_{ns}(\vec{k}) \quad . \tag{3}$$

In Eq. (3), $P_{ns}(\vec{k})$ is an appropriate dipole matrix element, and

$$\omega_{ns}(\vec{k}) = [E_n(\vec{k}) - E_s(\vec{k})]/\hbar \quad . \tag{4}$$

The quantity $\epsilon_2(\omega)$, of course, is a scalar for cubic crystals.

As previously set out, the energy integration is done with a Monte Carlo method in conjunction with a quadratic interpolation. The momentum matrix element can vary quite rapidly with $\vec{k}$ for a NFE metal in contrast with the slow variation characteristic of insulators. It is thus important to account for this in the calculation. Therefore, the 2000-point mesh is used for a quadratic interpolation of the matrix element. The result of using 1 100 000 points in the $\frac{1}{48}$th part of the zone is shown in Fig. 3.

The two peaks near 1.6 and 0.5 eV are striking. Since they are so prominent, it is extremely important to look for their origin in the band structure. It is apparent in the following discussion that they are a necessary by-product of the NFE picture for aluminum. The peak positions are sensitive to the potential, and the amplitudes are sensitive to E_F, but the existence of the structure is virtually guaranteed. Other workers have also noted the presence of these peaks.[19,20]

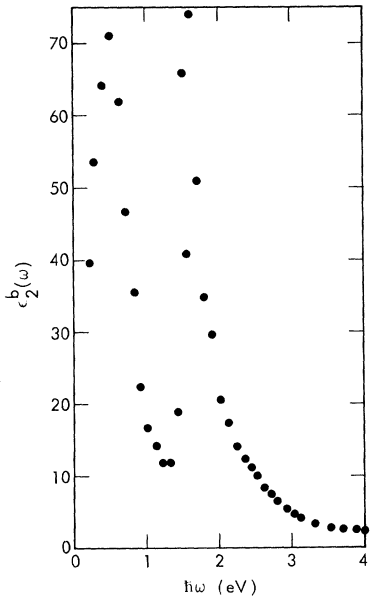

FIG. 3. Interband contribution $\epsilon_2^b(\omega)$ to the imaginary part of the dielectric function, neglecting lifetime broadening.

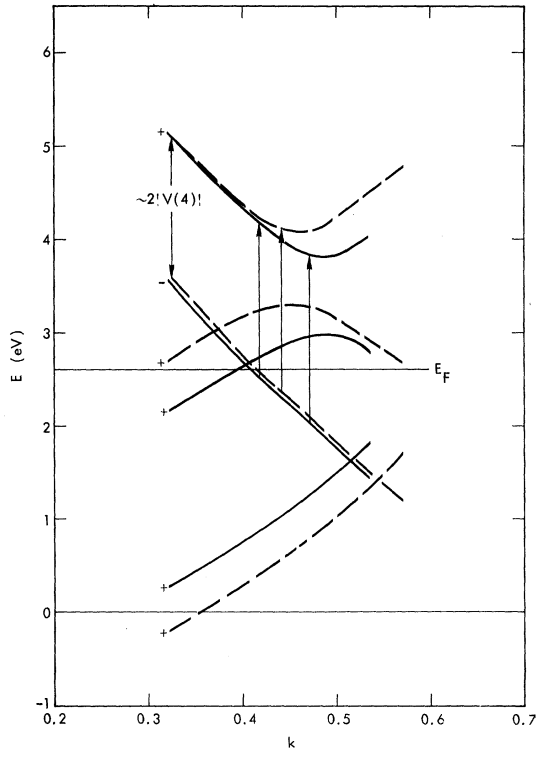

FIG. 4. Energy bands in the ΓXWK reflection plane of the Brillouin zone. The solid line refers to the locus (0.96, k, 0.0) and the dotted line to (0.93, k, 0.0). A plus sign indicates even parity vis-à-vis reflection in the plane, whereas a minus sign indicates odd parity. Some transitions contributing to the 1.6 eV in $\epsilon_2^b(\omega)$ are shown by arrows.

The origin of the 1.6-eV peak can be understood from an examination of Fig. 4. Some energy contours near the Fermi level are drawn for parallel lines in the ΓXWK reflection plane. Transitions contributing to the peak are sketched in. Not surprisingly, the bands are quite parallel near the Fermi level. This is quite simple to understand. In the completely free-electron picture, the plane waves $(\bar{1}, \bar{1}, \bar{1})$ and $(\bar{1}, \bar{1}, 1)$ are degenerate over the entire reflection plane (that is, the portion lying in the $\frac{1}{48}$th part of the zone under study). These two states are split by the $V(4)$ component of the potential. Thus, the band gap separating the resulting parallel bands is $\sim 2 \times |V(4)| = 1.54$ eV, and a sizable portion of the reflection plane contributes to the optical peak. Since we have strong mixing of states, a large dipole matrix element couples the initial and final states. (This is often called umklapp enhancement.) It is interesting to note in connection with this piece of structure that the transitions at the

W point are not particularly close to $\hbar\omega$ (peak) in the present calculation. In particular, $W_3 \rightarrow W_1 = 1.95$ eV and $W_{2'} \rightarrow W_1 = 0.89$ eV with $W_{2'} > E_F$. These transitions, therefore, are not related to the large optical peak.

The peak near 0.5 eV is understood in a similar fashion. One expects – and indeed finds – a peak in $\epsilon_2^b(\omega)$ near $2|V(3)| = 0.49$ eV. Both this peak and the preceding one are related to zone-boundary effects in an extended zone picture.

To conclude this section, it is appropriate to make some remarks concerning the limit $\hbar\omega \rightarrow 0$. Inspection of Fig. 5 makes it clear that interband transitions are expected for all frequencies as $\omega \rightarrow 0$. There is, therefore, no threshold frequency for the onset of interband transitions.

OPTICAL EFFECTIVE MASS

Although the pseudopotential is weak, there can still be considerable correction to the free-electron optical mass owing to the close proximity of the Fermi surface and the zone boundaries. The expression for the optical effective mass is, according to Cohen,[21]

$$\frac{1}{m_a^*} = \frac{1}{3N}\frac{1}{\hbar^2}\sum_{l',\vec{k}} \nabla_k^2 E_{l'}(\vec{k}) \quad , \tag{5}$$

where the sum is over all occupied levels, and N is the number of electrons per unit volume. In Eq. (5), m_a^* is the quantity that appears in the plasma frequency

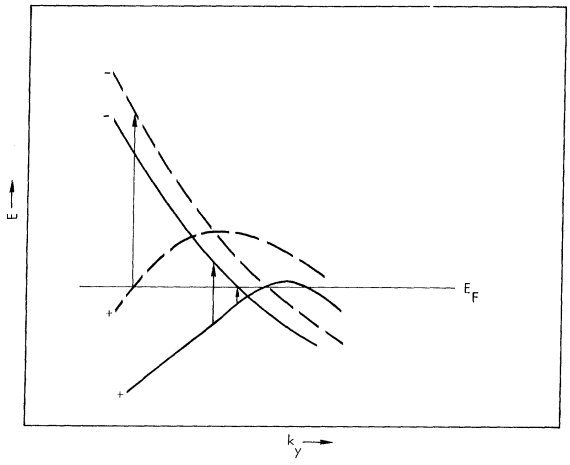

FIG. 5. Sketch of the energy bands along some directions in the ΓXWK plane similar to Fig. 4. Note that the crossing of bands occurs above the Fermi surface for the dotted lines, whereas it occurs below in the case of the solid lines. Therefore, these will be an intermediate line along which the bands cross at the Fermi level. This indicates an interband transition for which $\hbar\omega = 0.0$ eV.

$$\omega_p^2 = 4\pi N e^2/m_a^* \quad . \tag{6}$$

For the filled bands pertaining to the core states, the contribution to the summation in Eq. (5) vanishes. This then leaves us with three electrons per atom, and the electron density (N) in Eq. (5) refers to the valence electrons only.

One could attempt a direct evaluation of the second derivatives in Eq. (5), but this could be quite difficult for a NFE model. To see why consider the one-dimensional band structure in Fig. 6. Assuming the lower band to be full,

$$\frac{1}{\hbar^2}\sum_k \frac{d^2E}{dk^2} = 0 \quad .$$

Yet, $$\frac{1}{\hbar^2}\frac{d^2E}{dk^2} = \frac{1}{m_0}$$

over nearly the whole zone. There is a large negative curvature at the zone boundary that precisely cancels the positive contribution over the remainder of the zone. The negative part, being very large and localized to a small part of k space, would be hard to evaluate by a direct sampling procedure. [In the limit that $V(K) \rightarrow 0$, the negative spike becomes a delta function.] Similar difficulties are expected in the three-dimensional zone when there are occupied levels near zone boundaries.

To get m_a^* the following result is derived. Rewriting Eq. (1) slightly,

$$\epsilon_2^b(\omega) = \frac{1}{3}\frac{2\pi^2e^2}{m_0}\sum_{\vec{k}}\sum_{ll'}\frac{1}{\omega} f_{ll'}(\vec{k})\delta(\omega - \omega_{ll'}) \quad , \tag{7}$$

where now it is understood that l' runs over only occupied levels and l over unoccupied levels. Then using the well-known theorem,[22]

$$\sum_\alpha f_{\alpha l'}(\vec{k}) = 3 - (m_0/\hbar^2)\nabla^2 E_{l'}(\vec{k}) \quad , \tag{8}$$

where α runs over all values of the band index except l'. Then it follows that

$$\frac{1}{\hbar^2}\sum_{l'}\nabla^2 E_{l'}(\vec{k}) = \frac{1}{m_0}\sum_{l'}\left[3 - \sum_l f_{ll'}(\vec{k})\right] \quad , \tag{9}$$

where ll' has the meaning appropriate to Eq. (7). To establish Eq. (9), note that

$$f_{\alpha\beta} = -f_{\beta\alpha} \quad .$$

Therefore,

$$\frac{1}{\hbar^2}\sum_{kl'}\nabla^2 E_{l'}(\vec{k}) = \frac{1}{m_0}\left[3N - \sum_{\vec{k}ll'} f_{ll'}(\vec{k})\right] \quad , \tag{10}$$

where N is the number of electrons per unit of crystal volume and hence, the total number of occupied valence levels where due allowance has been made for the spin degeneracy.

From Eq. (7), we have

$$\int_0^\infty \epsilon_2^b(\omega)\omega\, d\omega = \frac{1}{3}\frac{2\pi^2e^2}{m_0}\sum_{kll'} f_{ll'}(\vec{k}) \tag{11}$$

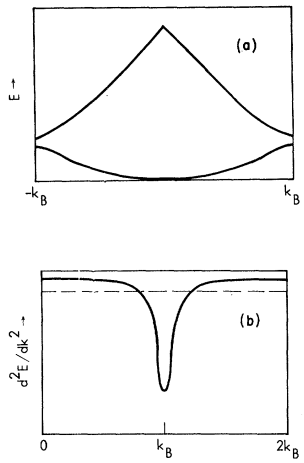

FIG. 6. (a) Nearly free-electron bands in one dimension; (b) the second derivative of the lower curve in (a).

and so

$$\frac{1}{\hbar^2}\sum_{kl'}\nabla^2 E_{l'}(\vec{k}) = \frac{1}{m_0}\left(3N - \frac{3m_0}{2\pi^2 e^2}\int_0^\infty \epsilon_2^b(\omega)\omega\, d\omega\right) \tag{12}$$

Finally,

$$m_0/m_a^* = 1 - m_0\int_0^\infty \epsilon_2^b(\omega)\omega\, d\omega/2\pi^2 Ne^2 \ . \tag{13}$$

This result is also known to follow from the sum rules.[13] It was necessary, however, to establish it as a result inherent in the band calculation before using it. Performing the calculation suggested by Eq. (13) gives $m_a^* = 1.45\ m_0$. This appears to be in excellent agreement with the experimental value of $1.50\ m_0$.[13]

Actually, Eq. (8) is only rigorously true for a local potential operator. Since we have a weak nonlocal term in the Hamiltonian, one should include this in the derivation of Eq. (13). From the form and magnitude of the nonlocal correction, one would expect about a 4% increase in m_a^*. This correction brings experiment and theory into exact agreement.

COMPARISON OF THEORY AND EXPERIMENT

In order to make contact with experiment, it is necessary to incorporate lifetime broadening. The interband contribution was calculated with several values of $\hbar/\tau = \frac{1}{2}\Gamma$. The approximation to the lifetime broadening function discussed elsewhere was used.[23] A constant value for the lifetime broadening is equivalent to taking the imaginary part of the self-energy function as independent of both energy and wave number. This may not be a bad approximation provided the scattering is phonon or impurity dominated rather than primarily due to electron-electron scattering. Since initial and final states are close to the Fermi surface, the density of states varies by less than a factor of 2 over the entire energy range.

The Drude contribution $\epsilon_2^f(\omega)$ is included by use of the equation[13]

$$\epsilon_2^f(\omega) = \frac{\omega_p^2/\tau}{\omega(\omega^2 + 1/\tau^2)} \ .$$

Taking the same value of τ in both the interband and intraband terms, and noting that $\epsilon_2(\omega) = \epsilon_2^b(\omega) + \epsilon_2^f(\omega)$, we have the results shown in Fig. 7. The 1.5-eV peak is apparent in all of the curves. The low-energy peak disappears into the free-electron background quickly when the lifetime is decreased. In Fig. 8, comparison is made between theory and experiment. The amplitude of our peak is a bit larger than experiment. Recent work[20] indicates, however, that our peak height is nearly correct for $\hbar/\tau = 0.132$ eV. In addition, it would appear that careful subtraction of the free-electron part of the dielectric function[20] discloses the presence of the 0.5 eV, which apparently also has the correct amplitude. In Fig. 9, we compare our results for $\sigma_1(\omega)$ with some recent low-temperature data.[24]

CONCLUSIONS

The present work seems to indicate that, for a simple polyvalent metal like aluminum, one can adequately calculate the optical response functions from the band structure. Furthermore, the same pseudopotential gives the Fermi surface.

It is pleasing that m_a^* is in good agreement

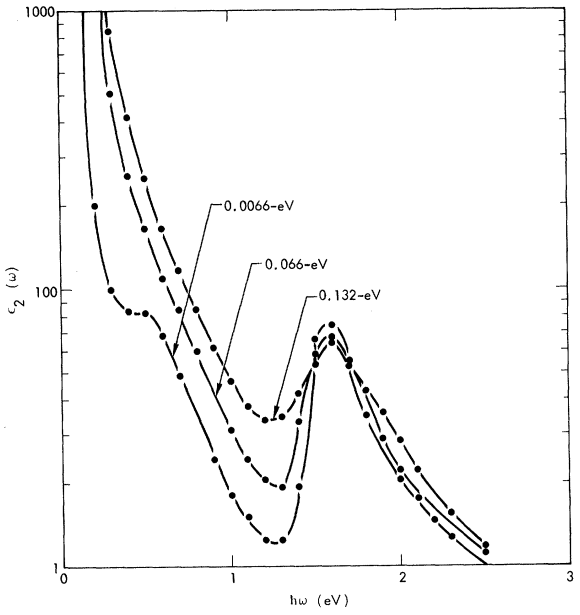

FIG. 7. The imaginary part of the dielectric function $\epsilon_2(\omega) = \epsilon_2^b(\omega) + \epsilon_2^f(\omega)$ for several values of $\hbar/\tau$ is shown to the left on the curves.

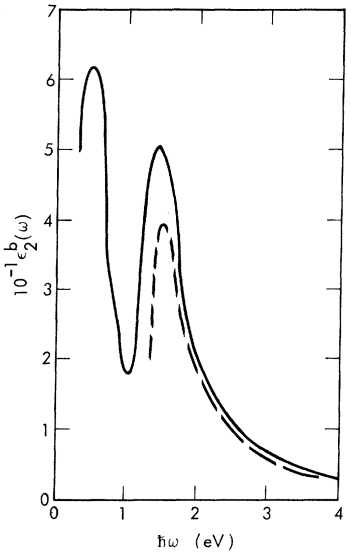

FIG. 8. Comparison of theory $\hbar/\tau = 0.132$ eV (solid line) with the experimentally determined result of Ehrenreich *et al.* for $\epsilon_2^b(\omega)$ (dashed line).

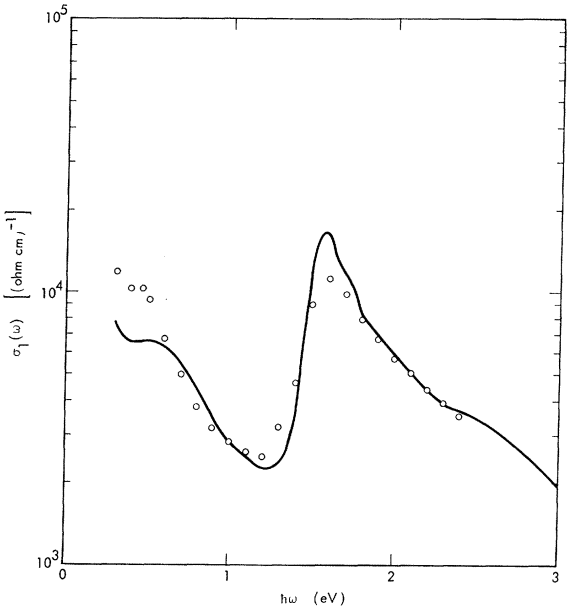

FIG. 9. Comparison of $\sigma_1(\omega)$ in $(\Omega\,\mathrm{cm})^{-1}$ with the low-temperature data of Lynch (Ref. 24). The open circles were taken from the experiment, and the solid line is theory with $\hbar/\tau = 0.02$ eV.

with experiment, particularly since Beeferman and Ehrenreich[25] have recently shown that the many-particle effects give only a weak shift of oscillator strength between the intraband and interband absorption. With respect to the Drude absorption, Powell[26] has recently criticized the use of frequency-independent parameters. Part of the difficulty with the Drude term probably arises from the presence of interband effects of greater intensity than expected.

Finally, we note that it might be interesting to examine the optical spectrum as a function of strain. A study of differential optical line shapes would, however, require a high resolution study such as has been done for semiconductors.[27] Nevertheless, given the optical peak positions, determination of the coefficients $V(3)$ and $V(4)$, is possible, and this information can be used in delineating the Fermi surface both at zero strain and at high pressure.

Note added in proof. It has previously been noted both by Harrison[28] and by Golovashkin *et al.*[29] that there should be interband peaks associated with the Fourier coefficients of the pseudopotential in Al.

ACKNOWLEDGMENTS

The author is grateful to Dr. Fred Wooten, Dr. Tony Huen, and Dr. Phillip Best for useful discussions. Thanks also to Dr. R.N. Keeler and Marvin Ross for reading the manuscript, Professor D. Beaglehole for helpful correspondence, and Professor D.W. Lynch for permission to use his experimental results prior to publication, as well as for useful conversations.

---

*Work performed under the auspices of the U.S. Atomic Energy Commission.

[1]W. A. Harrison, Phys. Rev. 118, 1182 (1960).

[2]N. W. Ashcroft, Phil. Mag. 8, 2055 (1963).

[3]L. G. Schulz and F. R. Tangherlini, J. Opt. Soc. Am. 44, 362 (1954).

[4]J. N. Hodgson, Proc. Phys. Soc. (London) B68, 593 (1955).

[5]J. R. Beattie and G. K. T. Conn, Phil. Mag. 46, 235 (1955).

[6]A. I. Golovashkin, G. P. Motulevich, and A. A. Shubin, Zh. Eksperim. i Teor. Fiz. 38, 51 (1960) [Soviet Phys. JETP 11, 38 (1960)].

[7]G. Hass and J. E. Waylonis, J. Opt. Soc. Am. 51, 719 (1961).

[8]H. E. Bennett, M. Silver, and E. J. Ashley, J. Opt. Soc. Am. 53, 1089 (1963).

[9]R. P. Madden, L. R. Canfield, and G. Hass, J. Opt. Soc. Am. 53, 620 (1963).

[10]I. N. Shkyarevskii and R. G. Yarovaya, Opt. i Spektroskopiya 14, 252 (1963) [Opt. Spectry. (USSR) 14, 130 (1963)]; 16, 85 (1964) [16, 45 (1964)].

[11]A. P. Lenham and D. M. Treherne, J. Opt. Soc. Am. 56, 752 (1966).
[12]G. Dresselhaus, M. S. Dresselhaus, and D. Beaglehole (unpublished).
[13]H. Ehrenreich, H. R. Philipp, and B. Segall, Phys. Rev. 132, 1918 (1963).
[14]B. Segall, Phys. Rev. 131, 121 (1963).
[15]M. Ross and K. W. Johnson (unpublished).
[16]A. O. E. Animalu and V. Heine, Phil. Mag. 12, 1249 (1965).
[17]V. Heine, Proc. Roy. Soc. (London) A240, 361 (1957).
[18]D. Brust, Phys. Rev. 134, A1337 (1964).
[19]A. J. Hughes, D. Jones, and A. H. Lettington, J. Phys. C 2, 102 (1969).
[20]G. Dresselhaus, M. S. Dresselhaus, and D. Beaglehole, Proceedings of the Electronic Density of States Conference, Gaithersburg, Maryland, 1969 (unpublished).
[21]M. H. Cohen, Phil. Mag. 3, 762 (1962).
[22]N. F. Mott and H. Jones, *The Theory of the Properties of Metals and Alloys* (Clarendon Press, Oxford, England, 1936).
[23]D. Brust and L. Liu, Phys. Rev. 154, 647 (1967).
[24]D. W. Lynch (unpublished).
[25]L. W. Beeferman and H. Ehrenreich, Bull. Am. Phys. Soc. 14, 397 (1969).
[26]C. J. Powell (unpublished).
[27]L. R. Saravia and D. Brust, Solid State Commun. 7, 669 (1969).
[28]W. A. Harrison, Phys. Rev. 147, 467 (1966).
[29]A. I. Golovashkin, A. I. Kopeliovich, and G. P. Motulevich, Zh. Eksperim. i Teor. Fiz. 53, 2053 (1968) [Soviet Phys. JETP 26, 1161 (1968)].

PHYSICAL REVIEW B VOLUME 2, NUMBER 4 15 AUGUST 1970

Gravitationally Induced Electric Field in Metals†

T. J. Rieger
Department of Physics, University of California, Santa Barbara, California 93106
(Received 30 October 1969)

The gravitationally induced electric field in a metal is calculated through the electron-phonon interaction. The field is of magnitude $\sim 10^{-6}$ V/m and is directed upward, in agreement with the results of Dessler *et al.* The electric field also exists inside superconducting materials, since once the field is decoupled, the electron-phonon interaction is essentially unchanged. This implies, of course, that other electron-phonon effects (e.g., resistivity) are unaffected by either the gravitational field or the induced electric field.

I. INTRODUCTION

Recently, there has been interest in an electric field in metals induced by a gravitational field. This interest divides between the related problems of a gravitationally induced electric field inside a metal and an induced field outside the surface of a metal. The situation is complicated, however, by the fact that the internal electric field is easier to calculate than the external field, which depends on the behavior of the surface dipole moment. On the other hand, measurement of the external field, although difficult, is easier than measurement of the internal field which is not readily accessible. This work is a calculation of the internal gravitationally induced electric field.

Attempts have been made to calculate the field outside a metal[1-3] and a inside metal.[2,4] Measurements of the field outside a metal have been attempted.[5-7] Schiff and Barnhill[1] obtained $mg/e \simeq 10^{-10}$ V/m directed downward for the field outside the metal, which is just the field required to screen out the gravitational force. In their analysis, however, they neglected the gravitational compression of the lattice. Dessler, Michel, Rorschach, and Trammel[2] recalculated the electric field including the elastic compression of the solid under its own weight, and related the change in density of the electron gas to the resulting density gradient of the ions. By requiring that the electrochemical potential of the electrons be constant, they derived the internal electric field necessary to balance the pressure gradient due to the inhomogeneous electron density. This is of strength $\sim 10^{-6}$ V/m and oppositely directed to the Schiff-Barnhill result. For the field outside the metal they obtained a similar result. Herring[3] considered the gravitationally induced electric field outside a body by carefully treating the surface stresses. He concluded that the larger Dessler *et al.* (DMRT) field exists outside a metal.

Still another, even simpler method, using the Fermi-Thomas model, has been suggested by Peshkin,[8] and leads to the DMRT field inside a metal.

In this analysis, a different method is used to